Mitigation of Large Power Spills by a Storage Device

Debarati Bhaumik, Daan Crommelin, and Bert Zwart

August 10, 2015

Abstract

The unpredictable nature of wind energy makes its integration to the electric grid highly challenging. However, these challenges can be addressed by incorporating storage devices (batteries) in the system. We perform an overall assessment of a single domestic power system with a wind turbine supported by an energy storage device. The aim is to investigate the best operation mode of the storage device such that the occurrence of large power spills can be minimized. For estimating the small probability of large power spills, we use the *splitting technique* for rare-event simulations. An appropriate *Importance Function* for splitting is formulated such that it reduces the work-load of the probability estimator as compared to the conventional Crude Monte Carlo probability estimator. Simulation results show that the *ramp constraints* imposed on the charging/discharging rate of the storage device plays a pivotal role in mitigating large power spills. It is observed that by employing a new charging strategy for the storage device large power spills can be minimized further. There exists a trade-off between reducing the large power spills versus reducing the average power spills.

1 Introduction

Integration of intermittent renewable sources of energy like solar and wind power into the electric grid has increased in recent times. The depletion of the exhaustible resources of energy and the strive for a carbon free future will enhance the usage of these renewable sources more. The unpredictable nature of the renewable energy sources lead to intermittent power generation. This makes the integration of renewable energy sources into the power grid a highly challenging task.

The adverse consequences of the intermittent power generation like load-shedding and power spills can be mitigated if the power system is supported by an energy storage device. The energy storage device acts as buffer energy source. It stores energy when there is over-generation of power, and delivers the stored energy to the system when there is under-generation of power.

Stand-alone systems with renewable generations like solar photovoltaic (PV) and wind supported with battery storage has been investigated in great detail with respect to the PV-wind generation sizing, performance, battery storage sizing, efficiency, optimization, system cost and reliability indices in [1]-[11].

Xu *et al.* in [12] investigated the feasibility of replacing diesel generation entirely with solar PV and wind turbines supplemented with energy storage by characterizing the load-shedding probabilities. Semaoui *et al.* in [13] recommended a model to optimize the sizes of battery capacity and PV generator for stand-alone PV system using two optimization criteria, the loss of power supply probability (LPSP) reliability criterion and energetic cost for economic evaluation. Cabral *et al.* analyzed loss of power supply (LPS) and LPSP for sizing the PV generators of stand-alone PV systems in [14]. Billinton *et al.* in [15] presented a simulation model for the reliability evaluation (loss of load expectation and loss of energy expectation) of small stand-alone wind energy conversion systems with respect to battery size, charging (discharging characteristics), wind speed, wind turbine characteristics etc. Casares *et al.* in [16] devised a mathematical methodology to predict Loss of Load Probability (LLP) for sizing stand-alone photovoltaic systems.

To improve the practical efficiency of renewable energy generation and to minimize the need of drastic actions (like using expensive fast ramping generators) to have uninterrupted power supply, it is important to store the excess power generated in the system. In this paper, we investigate a stand-alone single domestic power system with a local micro-generator wind turbine supplemented with an energy storage device. For this system we aim to answer the following question : what is the best way to operate the storage device (battery) such that the probability of large power spills is minimal? While most studies focus on the event where there is not enough supply of power to meet *consumer* demand, a large power spill is detrimental for the *producer*.

We use a simple energy balance method for the switching (charging/discharging) of the battery, i.e., when there is excess power generation the battery is charged and when there is deficit of power it is discharged. Such a simple switching strategy of the storage device has been considered in many previous studies on energy systems with renewable generations supplemented with storage devices, e.g. [9], [11]-[18].

To this end, we devise models for simulating the wind speeds and power demand such that the invariant probability densities of the data generated by the models are

comparable to the data from measurements. With these models for power generation and demand, we analyze how the *ramp constraints*, the imposed maximal charging/discharging rates on the storage device affects the probability of large power spills. And finally, we define a strategy for charging the storage device to reduce the probability of large power spills. It is expected that the new scheme for charging the storage device will increase the average power spill in a given time interval of interest. We study the trade-off between reducing the probability of large power spills and reducing the average power spilled by the system.

The probability of occurrence of large power spill is small. The Crude Monte Carlo (CMC) probability estimator is robust but becomes computationally highly intensive for small probabilities. To reduce the workload of CMC we use the *splitting technique* for rare-event simulations in our study [19]. We use a variant of the splitting technique called the Fixed Number of Successes (FNS) proposed by Amrein and Kunsch [20] for calculating the probability of large power spills. Wander *et al.* used FNS to estimate electrical grid reliability in [21]. It is of great relevance to find an appropriate *Importance Function* (IF) for the splitting technique, as it plays the most significant role in the efficiency of splitting [22]. We formulate an appropriate IF for our hybrid stochastic power system described above.

In section 2 we describe the set up of the system, the storage model, problem description and the stochastic models for power generation and demand. Section 3 provides details of the FNS splitting technique and the appropriate importance function for the problem. Section 4 presents the simulation results showing how the probability of large power spills vary with the battery parameters and charging strategy. In this section we also compare the CMC and FNS computation time. At the end Section 5 concludes the article.

2   System set up

In the single domestic power system with stochastic wind power generation and demand, a battery is incorporated as a storage device in order to reduce large power spills. Let $P(t)$ be the power mismatch between the wind power generation and demand (load) defined as

$$P(t) := W(t) - D(t), \qquad (1)$$

where $W(t)$ is the wind power generated and $D(t)$ is the power demand at time t. $P(t) > 0$ implies there is excess of power in the system and can be used to charge the energy storage device and $P(t) < 0$ denotes paucity of power in the system and the storage device needs to be discharged.

2.1   The storage model

Let us consider a battery as the energy storage device in the power system. The state of the battery at time t is given by $B(t)$ and it has a maximum storage capacity B_{max}. For any storage device there will be bounds on the rate at which it can be charged or discharged known as **ramp constraints** [23]. The ramp constraints are denoted as γ and β such that $\gamma < 0$ and $\beta > 0$. Losses occur during charging and discharging the battery which depends on the *efficiency parameter* α of the battery, where $0 < \alpha \leq 1$. The battery is modeled according to

$$\frac{dB}{dt} = \dot{B}(t) := \alpha P(t), \text{ for } t \in [0, T] \qquad (2)$$

with the *battery constraints*, namely the ramp and capacity constraints imposed on it

$$\gamma \leq \dot{B}(t) \leq \beta \quad \text{where } \gamma < 0 < \beta,$$
$$0 \leq B(t) \leq B_{max} \quad \forall \ t \in [0, T].$$

T is the time length of 24 hours. Thus, in principle, the battery is charged when $P(t) > 0$ and discharged if $P(t) < 0$ unless the battery constraints are met.

In our computational experiments, time is discretized into $N = \frac{T}{\Delta t}$ time steps, where Δt is the time step of integration. The battery state is updated according to the Euler scheme

$$B(t+1) = \min(B_{max}, \ \max(0, B(t) + \Delta B(t))), \qquad (3)$$

where

$$\Delta B(t) := \min(\beta, \ \max(\gamma, \alpha P(t)))\Delta t, \qquad (4)$$

for $t = 0, \ldots, N-1$. $B(0)$ is the initial state of the battery. If the battery is fully charged, $B(t) = B_{max}$, it will only discharge if $P(t) < 0$. Otherwise if $P(t) > 0$ it remains at B_{max} and vice-versa for the empty state of the battery, i.e., when $B(t) = 0$.

2.2   Power Spill

Let $\tilde{P}(t)$ be the amount of power getting absorbed or delivered by the battery,

$$\tilde{P}(t) = \begin{cases} \hat{P}(t) & \text{if } 0 < B(t) < B_{max}, \\ \hat{P}(t) & \text{if } B(t) = B_{max} \text{ and } P(t) < 0, \\ \hat{P}(t) & \text{if } B(t) = 0 \text{ and } P(t) > 0, \\ 0 & \text{otherwise,} \end{cases} \qquad (5)$$

where

$$\hat{P}(t) = \min(\beta, \max(\gamma, \alpha P(t))). \qquad (6)$$

Let us define the *residual power* as

$$F(t) := P(t) - \tilde{P}(t). \tag{7}$$

When $F(t) > 0$, **power spill** occurs: there is more power production than demand and the battery cannot absorb all the excess power because of the *battery constraints*, i.e., either the battery is completely charged or it cannot charge fast enough due to the ramp constraints. Note that power spill can also occur when $P(t)$ is large and $\alpha < 1$.

2.3 Problem description

We are interested in calculating the probability of large power spills in the system over a time length T, i.e.,

$$\mathcal{P}(\sup_{t \in [0,T]} \{F(t)\} \geq F^*), \tag{8}$$

where $F^* > 0$ is the large *power spill threshold*.

To make an overall assessment of the integrated system we compare how this probability varies for various values of B_{max}, the ramp constraints and for different battery charging schemes (see sections 4.1 and 4.2).

2.4 Modeling power mismatch $P(t)$

As discussed earlier we model the stochastic power mismatch $P(t)$ from (1) by modeling $W(t)$ and $D(t)$.

2.4.1 Wind power generation $W(t)$

Earlier studies have shown that the Rayleigh distribution (a special case of Weibull distribution with shape parameter equal to 2) arises from the wind speeds if the wind vector components u and v are taken to be individually independently Gaussian distributed with zero means and equal standard deviations. These assumptions may be suitable globally but certainly are not true in general locally [24]. We generalize the assumptions by taking u and v as independent (no cross-correlation) and Gaussian with *non-zero* means (μ_u and μ_v respectively) and different standard deviations (σ_u and σ_v respectively). μ_u and μ_v are the average wind velocities in the east-west and the north-south direction respectively. σ_u and σ_v are the standard deviations along the wind component directions. In [24], $\mu_v = 0$ and $\sigma_u = \sigma_v$. To get realistic values for the means and standard deviations of the wind velocity components, we use hourly wind data from KNMI [25]. The KNMI data consists of hourly measurements throughout 2013 of wind velocity at a height of 10 m at the Schiphol airport in the Netherlands. The Gaussian processes for the wind velocities are modeled as two 1-d Ornstein-Uhlenbeck processes,

$$dU(t) = \Theta_U(M_U - U(t))dt + \Sigma_U dW(t), \tag{9}$$

and

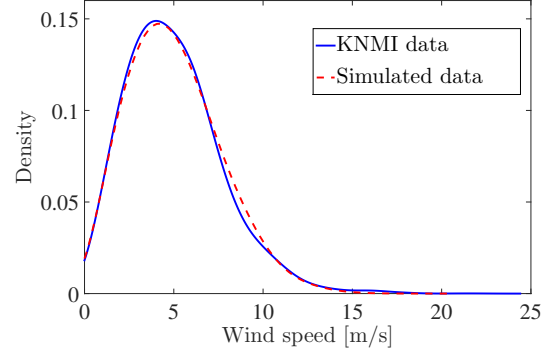$$dV(t) = \Theta_V(M_V - V(t))dt + \Sigma_V dW(t), \tag{10}$$

Figure 1: Comparing the approximated densities of KNMI and simulated wind speeds.

where $M_U = \mu_u$ and $M_V = \mu_v$; $\Sigma_U = \sqrt{2\Theta_U}\sigma_u$ and $\Sigma_V = \sqrt{2\Theta_V}\sigma_v$. The values of Θ_u and Θ_v are to be determined later (see section 2.4.3). The simulated wind speed is given by

$$W_s(t) = \sqrt{U^2(t) + V^2(t)}. \tag{11}$$

From Fig. 1 we observe that the model we use to generate the wind speeds are in good agreement with the KNMI measurement data.

The power produced by a wind turbine is a function of wind speed and can be modeled as [26]

$$W(t) = \begin{cases} W_{RP}\left[\frac{W_s(t) - W_{CI}}{W_{RS} - W_{CI}}\right] & \text{if } W_{CI} \leq W_s(t) \leq W_{RS}, \\ W_{RP} & \text{if } W_{RS} < W_s(t) < W_{CO} \\ 0 & \text{otherwise.} \end{cases} \tag{12}$$

Here, W_{RP} is the rated wind power, W_{CI} is the cut-in wind speed at which the turbine starts to generate, W_{RS} is the rated wind speed at which the turbine produces its rated power and W_{CO} is the cut-out wind speed at which the turbine shuts down for safety reasons. In our study we consider a micro-generator domestic wind turbine with $W_{RP} = 1100$ W, $W_{CI} = 2$ m/s, $W_{RS} = 10$ m/s and $W_{CO} = 18$ m/s. The turbine cannot generate output below a certain threshold of wind speed W_{CI}. Above the cut-out wind speed W_{CO} it needs to be shut down to avoid damage to the turbine.

From the density of wind power produced Fig. 2 we observe that there exist an upper and a lower bound on the power produced because of the physical restrictions on the wind turbine. The peak at zero is due to the turbine output being zero and the higher wind power peak is due to the turbine output being W_{RP}.

2.4.2 Power demand $D(t)$

The bar plot of Fig. 3 shows the density plot of the measured power consumption of a typical household for one year [27]. We observe that there exist two peaks in the
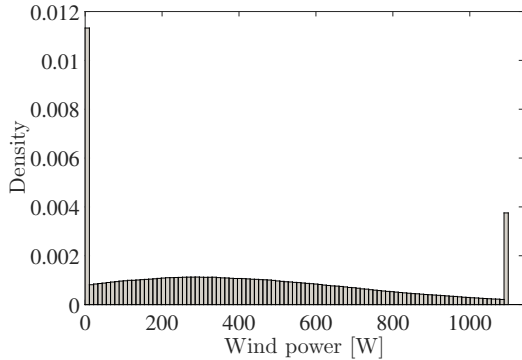
Figure 2: Density of the wind power produced for W_{CI}=2 m/s, W_{CO}=18 m/s, W_{RS}=10 m/s and W_{RP}= 1100 W.
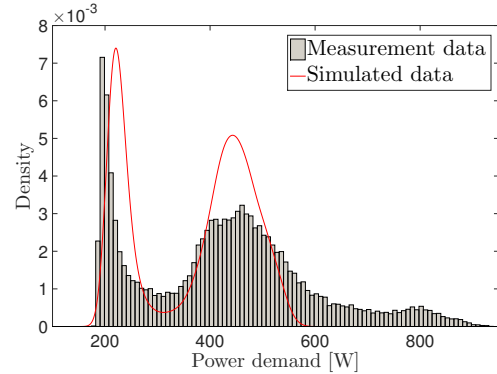

Figure 3: Comparison of the measured and the simulated data for the yearly electricity consumption of a typical household.

Table 1: Polynomial constants for $V(D) \approx \sum_i^7 a_i D^{7-i}$.

i	a_i
1	0.1977
2	-1.1643
3	1.9195
4	0.6014
5	-3.2804
6	0.5133
7	-5.3003

Figure 4: Comparing the ACF of the simulated wind and demand data with KNMI wind speed data.

density plot, one is the night-time peak at the lower power value, the other is the high valued peak at day-time. We model the power demand by the following SDE which mimics the day-time and night-time peaks,

$$dD(t) = -\frac{V'(D(t))}{c}dt + \frac{1}{\sqrt{c}}dW(t), \qquad (13)$$

where $V(D(t))$ is the so-called potential function for $D(t)$ and c is a constant to be determined later (see section 2.4.3). The relation between the invariant probability density $\psi(D)$ and the potential function $V(D(t))$ for (13) is given by

$$\psi(D) = \psi_0 \exp(-V(D)), \qquad (14)$$

where ψ_0 is a constant. The potential function $V(D)$ was obtained from the density distribution of the measured load data by inverting (14)

$$V(D) = -\log\psi(D) + \log\psi_0. \qquad (15)$$

In order to obtain an expression for the potential, a 6th order polynomial was fitted on the values of $V(D)$ calculated from (15). In order to avoid ill-conditioned values for the polynomial constants, the demand data was rescaled by a factor of 100 and re-centered by 300 W, i.e., $D_{\text{re-scaled}} = \frac{D-300}{100}$.

Fig. 3 shows the comparison of the density function of the simulated data and the measured data. We can
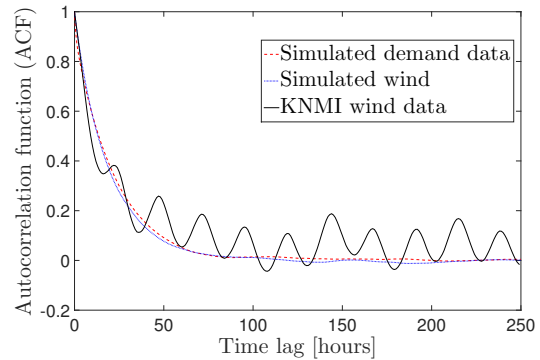
see that our power demand model captures the daytime and night-time peaks reasonably well. However, the demand model does not capture values greater than 600 W. This is because of the order of the polynomial chosen for $V(D(t))$. In this study we neglect the periodic switching between the day-time and night-time peaks in this model and consider random switching between the peaks.

2.4.3 Auto-correlation function (ACF)

The choice of Θ_U, Θ_V and c for (9), (10) and (13) is crucially important so that all the simulated data decorrelate at a comparable time with the KNMI wind data (see Fig. 4). To achieve this, we take $\Theta_U = \Theta_V = 0.025$ and $c = 2$.

2.4.4 Power mismatch

The power mismatch between the generation and demand is given by

$$P(t) = W(t) - D(t). \qquad (16)$$

We observe four maxima in the density of power mismatch in Fig. 5. These maxima occur when the power generated
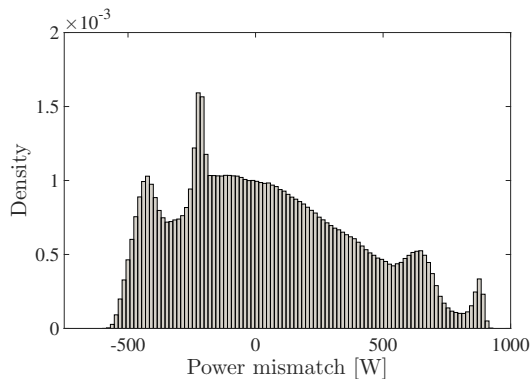
4

Figure 5: Density plot of power mismatch between power generation and power demand.

$G(t)$ is minimum or maximum and the day-time or night-time peaks occur.

From the wind and demand models discussed in this section we calculate the probability of large power spills (8) when a battery is incorporated into the system.

3 Rare event simulation : Fixed number of successes splitting technique

In our model we are interested in estimating probabilities of large power spills when a battery is incorporated in a power system with stochastic power generation and demand. It is expected that the probability of large power spills will be small when a battery is incorporated in the system. The Crude Monte Carlo (CMC) estimations of these small probabilities will become computationally very expensive.

3.1 A review of the splitting technique

We now give a review of the rare event simulation technique we follow [19]. Let $(\Omega, \mathcal{F}, \mathcal{P})$ be a probability space and $A \in \mathcal{F}$ be the rare event of interest. If A is a rare event, it implies $\gamma = \mathcal{P}(A)$ is small. The CMC estimator of $\mathcal{P}(A)$ is given by

$$\tilde{\gamma} := \frac{1}{M} \sum_{j=1}^{M} \mathbb{1}_{\{A \text{ occurs in sample j}\}}, \qquad (17)$$

where M is the number of samples generated.

The *squared relative error* of the CMC estimator (17) is given by

$$\text{SRE}(\tilde{\gamma}) := \frac{\text{Var}(\tilde{\gamma})}{\gamma^2} = \frac{\gamma(1-\gamma)/M}{\gamma^2} = \frac{1-\gamma}{\gamma M}. \qquad (18)$$

For fixed M, the SRE diverges as $\gamma \to 0$. Hence, CMC becomes unreliable when γ is small. Otherwise to achieve

an acceptable SRE we need very large values of M. For example, to estimate probabilities smaller than 10^{-4} one needs $M \gtrsim 10^6$ CMC samples for achieving SRE ≈ 0.01.

To reduce the computational workload for estimating $\tilde{\gamma}$ we use a rare event simulation technique called *splitting* [28]. More precisely, we use the Fixed Number of Successes (FNS) version of splitting proposed by Amrein and Kunsch [20]. In splitting, the sample paths of the stochastic processes involved are split into multiple copies at various levels of the *Importance Function* (IF) till the rare event set is reached. The IF measures the distance of the rare-event set. The probability γ is decomposed into the product of several conditional probabilities which occur more easily and are hence less computationally intensive to calculate.

Let $\mathbf{X}$ be a vector-valued Markov process with state space ξ

$$\mathbf{X}(t) := (X_1(t), \cdots, X_n(t)), \text{ for all } t \geq 0.$$

The major hurdle for splitting is to find an appropriate IF ϕ

$$\phi(\mathbf{X}(t)) : \xi \longrightarrow \mathbb{R}, \qquad (19)$$

which assigns importance values to $\mathbf{X}(t)$. Let $A_{\phi,L,t}$ be the rare event set defined in terms of ϕ as

$$A_{\phi,L,t} = \{\mathbf{X}(t) \in \xi : \phi(\mathbf{X}(t)) \geq L\}.$$

We are interested in the rare event

$$A = \{\exists t \leq T : A_{\phi,L,t} \text{ holds}\}. \qquad (20)$$

For the splitting technique we split the interval $[0, L]$ into m sub-intervals with boundaries $0 = l_0 < l_1 < \cdots < l_m = L$. We define $T_k = \inf\{t > 0 : \phi(\mathbf{X}(t)) \geq l_k\}$ as the time of hitting the k-th level and $H_k = \{T_k < T\}$ as the event that the k-th level is hit during $[0, T]$. Therefore, $\gamma = \mathcal{P}(H_m)$ and $\mathcal{P}(H_0) = 1$. As $H_m \subset H_{m-1} \subset \cdots \subset H_1 \subset H_0$, we have

$$\gamma = \mathcal{P}(A) = \prod_{k=1}^{m} \mathcal{P}(H_k|H_{k-1}) = \prod_{k=1}^{m} p_k,$$

where $p_k := \mathcal{P}(H_k|H_{k-1}) = \mathcal{P}(H_k)/\mathcal{P}(H_{k-1})$. Each p_k is estimated separately by generating independent sample paths from the distribution of the entrance state $G_{k-1} := (T_{k-1}, \mathbf{X}(T_{k-1}))$ conditioned on H_{k-1} at the threshold level l_{k-1}. The empirical distribution $\hat{G}_k$ is an estimate of the entrance distribution G_k which is obtained from H_k. Thus we can proceed recursively, replacing $\hat{G}_{k-1}$ for G_{k-1} and estimate p_k at each level k by the proportion of level hits

$$\hat{p}_k = R_k/N_{k-1} \text{ for all } R_k > 0, \qquad (21)$$

with R_k are the number of sample paths where H_k occurs and N_k is the total number of sample paths at level k. γ is estimated by the product of $\hat{p}_k$'s :
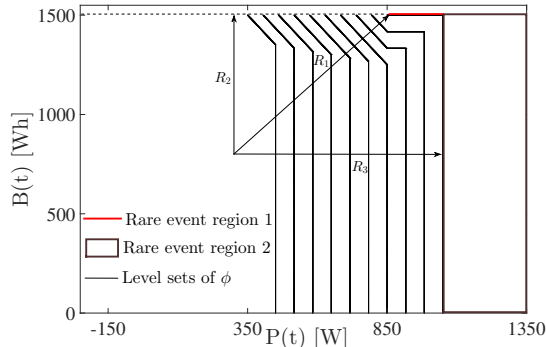
Figure 6: The phase space of $B(t)$ and $P(t)$, where $B_{max} = 1500$ Wh, $F^* = 850$ W and $\beta = 200$ W

$$\prod_{k=1}^{m} \hat{p}_k = \prod_{k=1}^{m} \frac{R_k}{N_{k-1}}. \tag{22}$$

For the FNS splitting technique [20] we keep the number of hits per level R_k fixed. The process is independently repeated by selecting an entrance state at random and simulating the process from the selected state upto $\min\{T_k, T\}$ until R_k hits are observed. In this method path extinction or explosion is avoided but the computation effort is compromised. The unbiased estimator of the rare-event probability is given by

$$\hat{\gamma} := \prod_{k=1}^{m} \tilde{p}_k = \frac{R_k - 1}{N_{k-1} - 1}. \tag{23}$$

The unbiased estimator for the variance $\text{Var}(\hat{\gamma})$ is not known for the FNS method. However, under the assumption that the conditional hitting probability does not depend on the entrance states of the previous stage,

$$\mathcal{P}(H_k | H_{k-1}, (T_{k-1}, \mathbf{X}(T_{k-1}))) = \mathcal{P}(H_k | H_{k-1})$$
$$(\forall (T_{k-1}, \mathbf{X}(T_{k-1})), \forall k),$$

the squared relative error of $\hat{\gamma}$ can be bounded :

$$\text{SRE}(\hat{\gamma}) \leq \prod_{k=1}^{m} \left(\frac{1}{R_k - 2} + 1 \right) - 1. \tag{24}$$

3.2 Importance function for the stochastic domestic power system

The IF plays a pivotal role in the efficiency of splitting [22]. In this section we present an appropriate IF function for the stochastic power system with a battery incorporated. We define the *importance function* ϕ as the distance of the system from the rare event sets in the phase space of the state of battery $B(t)$ and the power mismatch $P(t)$.

For formulating the IF, we define three ℓ_1 (or Manhattan) distances from the rare event sets (see Fig. 6) as

$$R_1(P(t), B(t)) = a_1(F^* - P(t)) + a_2(B_{max} - B(t)),$$
$$R_2(P(t), B(t)) = a_2(B_{max} - B(t)),$$
$$R_3(P(t), B(t)) = a_3(F^* + \beta - P(t)),$$

where, $a_1 = 1/F^*$, $a_2 = 1/B_{max}$ and $a_3 = 1/(F^* + \beta)$.

We define the importance function as

$$\phi(B(t), P(t)) = \begin{cases} -\min(R_1(P(t), B(t)), R_3(P(t), B(t))) \\ \qquad \text{if } P(t) < F^*, \\ -\min(R_2(P(t), B(t)), R_3(P(t), B(t))) \\ \qquad \text{if } P(t) \geq F^*. \end{cases} \tag{25}$$

The negative sign makes ϕ an increasing function in its arguments.

Fig. 6 depicts the level sets of the IF ϕ and the rare-event sets in the phase space of the battery state $B(t)$ and the power mismatch $P(t)$. Power spill occurs when $P(t) > 0$ and the battery cannot absorb all the excess power because of the *battery constraints*, i.e., either the battery is completely charged or it cannot charge fast enough due to the ramp constraints. Our problem as discussed in section 2.3 is to find the probability of large power spills , i.e., when $F(t) \geq F^*$, where $F^* > 0$. *Rare event region 1* occurs when the battery is charged to its maximum capacity B_{max} and $P(t) \geq F^*$. *Rare event region 2* occurs when the battery cannot absorb all the power available to it because of the ramp constraints imposed on it and the residual power left is spilled. This happens when $P(t) \geq F^* + \beta$.

For splitting, we construct the levels sets of the IF ϕ such that it depicts the distance of the system state from the rare event sets. From (8) and (25) we have

$$\hat{\gamma} := \mathcal{P}(\sup_{t \in [0,T]} \{F(t)\} \geq F^*) =$$
$$\mathcal{P}(\sup_{t \in [0,T]} \{\phi(B(t), P(t))\} \geq 0). \tag{26}$$

4 Results and Discussion

In this section, we discuss how the probability of power spills (beyond a threshold) varies with the battery size, ramp constraint imposed on the battery and for different charging scheme of the battery. We integrate (2), (9), (10), and (13) using forward Euler integration scheme with time step $\Delta t = 0.01$ hours and $T = 24$ hours. For all the calculations we take the initial state of the battery $B(0) = B_{max}/2$. For simplicity we use $\gamma = -\beta$ and the *efficiency parameter* $\alpha = 1$, as it does not add any new character to the structure of the model [23]. We calculate the probability of power spills greater than 850 W, i.e., $F^*=850$.

For performing FNS we first calculate the number of levels m by the pilot run such that $\tilde{p}_k$ is nearly equal to
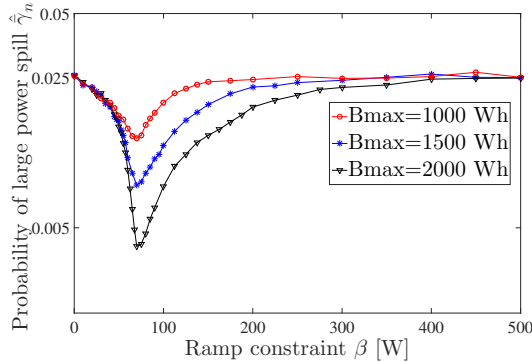
Figure 7: Probability of large power spill versus ramp constraint with F^*=850 W and T= 24 hours for various storage capacities.

Figure 8: Probability of large power spill versus ramp constraint β with B_{max}=1500 Wh, F^*=850 W and T= 24 hours for various values of ϵ.

the optimal value of $p_{opt} \approx 0.2032$ [20]. For the pilot run we use $R_k = 50$ for all k. For the final run we calculate R_k from (24) such that the $SRE(\hat{\gamma}) \leq 0.01$. In order to obtain an accurate estimate of the probabilities, FNS is repeated $n \geq 30$ times (suggested by [29]) to calculate the mean of the estimator

$$\hat{\bar{\gamma}}_n := \frac{1}{n}\sum_{i=1}^{n}\hat{\gamma}_i. \tag{27}$$

We are interested in the squared relative error of the mean given by

$$SRE(\hat{\bar{\gamma}}_n) := \frac{1}{n}SRE(\hat{\gamma}_i). \tag{28}$$

To obtain the value of n we first repeat FNS 30 times, and it is repeated further until the $SRE(\hat{\bar{\gamma}}_n) \leq 0.005$.

4.1 Probability of large power spills for different values of B_{max} and β

We study the effect of the ramp constraint β on the probability of large power spills $\hat{\bar{\gamma}}_n$ for various battery capacities B_{max}. Fig. 7 shows how $\hat{\bar{\gamma}}_n$ varies with β for various values of B_{max}. We observe that $\hat{\bar{\gamma}}_n$ reduces with β till an optimal value β^* where it is minimal, then again increases and becomes constant. This means that, either a very fast or a very slow charging/discharging battery accounts for more large power spills. A very fast charging/discharging battery will get to its maximum capacity very soon; hence won't be able to store any excess power generated which will account for the large power spills. On the other hand, a very tightly constrained battery (small β) cannot absorb all the excess power in the system and power is spilled.

In terms of the phase space (see Fig. 6), for small values of β the system hits the *rare event region 2* and for $\beta > \beta^*$ the system hits *rare event region 1*.

We observe that for very small values of β there is no effect of the battery size B_{max} on the $\hat{\bar{\gamma}}_n$. This is because when the battery is very restricted it never gets charged
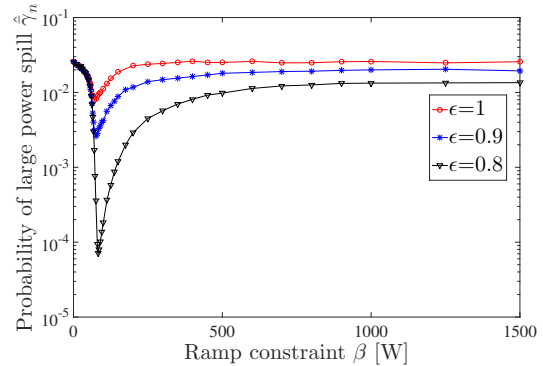
to its maximum capacity, hence B_{max} does not affect the probabilities. As β approaches β^* we see the effects of B_{max}: it reduces $\hat{\bar{\gamma}}_n$, which is expected. The larger the value of B_{max}, the longer it will take the battery to reach region 1. When β is very large the effect of B_{max} becomes negligible because the battery reaches it maximum capacity very fast and any excess power in the system greater than F^* lead to large power spills.

4.2 Probability of large power spills for different battery charging strategies

In order to reduce the large power spills further, we employ a different charging strategy for the battery. A fraction of the battery $1 - \epsilon$ is reserved for absorbing only those values of excess power which are greater than a threshold, where $0 \leq \epsilon \leq 1$. In our case we take the threshold same as the *power spill threshold* F^*. The battery is charged till :

1. ϵB_{max} if $P(t) < F^*$
2. B_{max} if $P(t) \geq F^*$.

The amount of power absorbed/ delivered by the battery is

$$\tilde{P}(t) = \begin{cases} 0 & \text{if } B(t) = \epsilon B_{max} \text{ and } 0 < P(t) < F^*, \\ 0 & \text{if } B(t) = B_{max} \text{ and } P(t) > 0, \\ 0 & \text{if } B(t) = 0 \text{ and } P(t) < 0, \\ \hat{P}(t) & \text{otherwise,} \end{cases}$$

where $\hat{P}(t) = \min(\beta, \max(\gamma, \alpha P(t)))$. We compare the probability of large power spills $\hat{\bar{\gamma}}_n$ for different ϵ.

Fig. 8 shows $\hat{\bar{\gamma}}_n$ versus β with $B_{max} = 1500$ Wh, F^* = 850 W and $T = 24$ hours for various values of ϵ. We observe that as the value of ϵ reduces, that is, as we reserve the battery more for larger fluctuations in $P(t)$, $\hat{\bar{\gamma}}_n$ decreases. This happens because of the reserved space
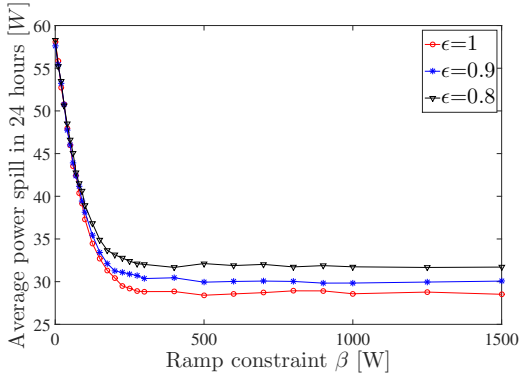
Figure 9: Average power spill power spill versus ramp constraint β with $B_{max} = 1500$ Wh, $F^* = 850$ W and $T = 24$ hours for various values of ϵ.

Table 2: Comparing the computation time for CMC and FNS for $B_{max}= 1500$ W, $\epsilon= 0.8$, $F^*= 850$ W and $n=30$. $\bar{\gamma}_n$ is the mean of the probability estimator for the estimation methods used.

β		CMC	FNS
40	$\bar{\gamma}_n$	1.81×10^{-2}	1.81×10^{-2}
	CPU time(s)	1×10^3	1.24×10^2
75	$\bar{\gamma}_n$	3.61×10^{-4}	3.60×10^{-4}
	CPU time(s)	2.55×10^4	4.33×10^2
85	$\bar{\gamma}_n$	7.11×10^{-5}	7.12×10^{-5}
	CPU time(s)	1.51×10^5	5.52×10^2

accessible to the battery only for absorbing the large values of $P(t)$. We observe similar response of the system to β as Fig. 7. From Fig. 8 we observe that the minimum value of $\hat{\bar{\gamma}}_n$ drops by a factor of 1000 from $\epsilon = 1$ to $\epsilon = 0.9$. So, the more we reserve the battery for large power mismatch, the lower will the probability of large power spills $\hat{\bar{\gamma}}_n$ become.

4.3 Average power spill

In the previous section 4.2 we observe that, if we reserve the battery for larger fluctuations in the net power mismatch, i.e., as ϵ decreases, the probability of large power spills $\hat{\bar{\gamma}}_n$ goes down drastically. But this increases the probability of small power spills. In this section we examine the time average of power spilled by the system over 24 hours versus β for different values of ϵ

$$\langle [F(t)]^+ \rangle_T = \frac{1}{T} \int_0^T [F(t)]^+ dt, \qquad (29)$$

where $[x]^+ := \max(0, x)$.

Fig. 9 shows the average power spill over a 24 hours of time interval versus β with $B_{max} = 1500$ Wh and $F^* = 850$ W for different ϵ. We observe that, the more we reserve the battery for the large values of $P(t)$, the higher the average power spill becomes. This happens because, when the battery state reaches ϵB_{max} it can further charge to its maximum capacity only if $P(t) \geq F^*$ and net power generated $P(t) < F^*$ is spilled. Hence, we observe increased average power spill.

4.4 CMC versus FNS

We compare the computation time for CMC and FNS probability estimator such that the squared relative error for both the methods are comparable, i.e, SRE($\tilde{\gamma}$) $\approx$ SRE($\hat{\gamma}_i$). Table 2 compares the computation time of CMC and FNS for few values of the probability of large power spill. As the value of the probability of large power

spills goes down the time gain of FNS over CMC becomes more profound. The simulations are performed using MATLAB 2012b on an Intel Core 2.50 GHz.

5 Conclusion

In our assessment for finding the best design to operate the storage device in a single domestic power system with wind generation for the simple switching strategy of the battery, we observe that the ramp constraints imposed on the battery play a major role in mitigating the large power spills. It is counter-intuitive to find that a fast charging/discharging battery is not beneficial for the system and results in large power spills more frequently. Increasing the storage capacity B_{max} reduces the probability of large power spill only when the battery operates around the optimal values of the ramp constraint β.

We employed a different charging scheme to the battery where a certain part of it is reserved only for absorbing large values of excess power in the system. We found that the probability of large power spills goes down significantly with the reserve level (see Fig. 8). But this charging scheme comes with a trade-off. The more we reserve the battery for larger fluctuations in the excess power generated, the higher the average power spill becomes, as depicted in Fig. 9. It should be noted that there is a nominal increase in the average power spill with ϵ, whereas the probability of the large power spills decreases drastically with ϵ.

We formulated the importance function for the FNS splitting technique used to calculate the probability of large power spills for our system. Table 2 shows the time efficiency of FNS over CMC. The time gain of FNS over CMC becomes more evident as the probability of interest becomes smaller.

References

[1] Zhou, Wei, et al. "Current status of research on optimum sizing of stand-alone hybrid solarwind power

generation systems." Applied Energy 87.2 (2010): 380-389.

[2] Yang, Hongxing, Lin Lu, and Wei Zhou. "A novel optimization sizing model for hybrid solar-wind power generation system." Solar energy 81.1 (2007): 76-84.

[3] Li, Chun-Hua, et al. "Dynamic modeling and sizing optimization of stand-alone photovoltaic power systems using hybrid energy storage technology." Renewable Energy 34.3 (2009): 815-826.

[4] Markvart, Tomas. "Sizing of hybrid photovoltaic-wind energy systems." Solar Energy 57.4 (1996): 277-281.

[5] Yang, Hongxing, et al. "Optimal sizing method for stand-alone hybrid solarwind system with LPSP technology by using genetic algorithm." Solar energy 82.4 (2008): 354-367.

[6] Al Badwawi, Rashid, Mohammad Abusara, and Tapas Mallick. "A Review of Hybrid Solar PV and Wind Energy System." Smart Science 3.3 (2015): 127-138.

[7] Barton, John P., and David G. Infield. "Energy storage and its use with intermittent renewable energy." Energy Conversion, IEEE Transactions on 19.2 (2004): 441-448.

[8] Ekren, Orhan, and Banu Y. Ekren. "Size optimization of a PV/wind hybrid energy conversion system with battery storage using simulated annealing." Applied Energy 87.2 (2010): 592-598.

[9] Prasad, A. Rajendra, and E. Natarajan. "Optimization of integrated photovoltaicwind power generation systems with battery storage." Energy 31.12 (2006): 1943-1954.

[10] Shakib, Arefeh Danesh, and Gerd Balzer. "Energy storage design and optimization for power system with wind feeding." Probabilistic Methods Applied to Power Systems (PMAPS), 2010 IEEE 11th International Conference on. IEEE, 2010.

[11] Wang, Caisheng, and M. Hashem Nehrir. "Power management of a stand-alone wind/photovoltaic/fuel cell energy system." Energy Conversion, IEEE Transactions on 23.3 (2008): 957-967.

[12] Xu, Huan, et al. "Load-shedding probabilities with hybrid renewable power generation and energy storage." Communication, Control, and Computing (Allerton), 2010 48th Annual Allerton Conference on. IEEE, 2010.

[13] Semaoui, Smail, et al. "Optimal sizing of a stand-alone photovoltaic system with energy management in isolated areas." Energy Procedia 36 (2013): 358-368.

[14] Cabral, Claudia Valria Tvora, et al. "A stochastic method for stand-alone photovoltaic system sizing." Solar Energy 84.9 (2010): 1628-1636.

[15] Billinton, R., and Y. Cui. "Reliability evaluation of small stand-alone wind energy conversion systems using a time series simulation model." Generation, Transmission and Distribution, IEE Proceedings. Vol. 150. No. 1. IET, 2003.

[16] Casares, F. J., et al. "Mathematical approach to the characterization of daily energy balance in autonomous photovoltaic solar systems." Energy 72 (2014): 393-404.

[17] Fragaki, Aikaterini, and Tom Markvart. "System memory effects in the sizing of standalone PV systems." Progress in Photovoltaics: Research and Applications 21.4 (2013): 724-735.

[18] Blchle, Max, et al. "Optimizing Neighborhood Consumption of Renewables through Clustering and H2 Storage: An Economic Assessment of an Austrian Community." International Conference on European Energy Market (2015)

[19] Rubino, Gerardo, and Bruno Tuffin, eds. "Rare event simulation using Monte Carlo methods." John Wiley & Sons, 2009.

[20] Amrein, Michael, and Hans R. Knsch. "A variant of importance splitting for rare event estimation: Fixed number of successes." ACM Transactions on Modeling and Computer Simulation (TOMACS) 21.2 (2011): 13.

[21] Wadman, Wander, Daan Crommelin, and Jason Frank. "Applying a splitting technique to estimate electrical grid reliability." Proceedings of the 2013 Winter Simulation Conference: Simulation: Making Decisions in a Complex World. IEEE Press, 2013.

[22] Garvels, Marnix Joseph Johann. "The splitting method in rare event simulation." Universiteit Twente, 2000.

[23] Gibbens, R. J., and F. P. Kelly. "Statistical aspects of storage systems modelling in energy networks." Information Sciences and Systems (CISS), 2012 46th Annual Conference on. IEEE, 2012.

[24] Monahan, Adam Hugh. "The probability distribution of sea surface wind speeds. Part I: Theory and SeaWinds observations." Journal of Climate 19.4 (2006): 497-520.

[25] KNMI, "Hourly data of the weather in the Netherlands," http://www.knmi.nl/klimatologie/uurgegevens/selectie.cgi, 2014, accessed September, 2014.

[26] Munteanu, Iulian, et al. *"Optimal control of wind energy systems: towards a global approach."* Springer Science & Business Media, 2008.

[27] EDSN, *"Hourly comsumption profile of a typical household,"* http://www.edsn.nl/verbruiksprofielen/, 2015, accessed February, 2015.

[28] Garvels, Marnix Joseph Johann. *"The splitting method in rare event simulation."* Universiteit Twente, 2000.

[29] Freund, John E., and Gary A. Simon. *"Modern elementary statistics."* Vol. 12. Englewood Cliffs, NJ: Prentice-Hall, 1973.